

X-ray Analysis of the Eccentric O-star Binary Iota Orionis 1

2000

Coordinated Monitoring of the Eccentric O-star Binary Iota Orionis: The X-ray Analysis

Julian M. Pittard^{1,2}, Ian R. Stevens¹, Michael F. Corcoran³, Ken G. Gayley⁴,
Sergey V. Marchenko⁵, Gregor Rauw^{1,6*}

¹*School of Physics and Astronomy, University of Birmingham, Edgbaston, Birmingham B15 2TT, UK*

²*School of Physics and Astronomy, University of Leeds, Woodhouse Lane, Leeds LS2 9JT, UK*

³*Universities Space Research Association/Laboratory for High Energy Astrophysics, GSFC, Greenbelt, MD 20771, USA*

⁴*University of Iowa, Iowa City, IA 52245, USA*

⁵*Département de physique, Université de Montréal, C.P. 6128, Succursale Centre-Ville, Montréal, Québec, H3C 3J7, Canada*

⁶*Institut d'Astrophysique & Géophysique, Université de Liège, 5, Avenue de Coïnte, B-4000 Liège, Belgium*

email: jmp@ast.leeds.ac.uk, irs@star.sr.bham.ac.uk, corcoran@barnegat.gsfc.nasa.gov, kgg@astro.physics.uiowa.edu,

sergey@astro.umontreal.ca, rauw@astro.ulg.ac.be

Accepted Received; in original form ...

ABSTRACT

We analyse two *ASCA* observations of the highly eccentric O9 III + B1 III binary Iota Orionis obtained at periastron and apastron. Based on the assumption of a strong colliding winds shock between the stellar components, we expected to see significant variation in the X-ray emission between these phases. The observations proved otherwise: the X-ray luminosities and spectral distributions were remarkably similar. The only noteworthy feature in the X-ray data was the hint of a proximity effect during periastron passage. Although this ‘flare’ is of relatively low significance it is supported by the notable proximity effects seen in the optical (Marchenko et al. 2000) and the phasing of the X-ray and optical events is in very good agreement. However, other interpretations are also possible.

In view of the degradation of the SIS instrument and source contamination in the GIS data we discuss the accuracy of these results, and also analyse archival *ROSAT* observations. We investigate why we do not see a clear colliding winds signature. A simple model shows that the wind attenuation to the expected position of the shock apex is negligible throughout the orbit, which poses the puzzling question of why the expected $1/D$ variation (i.e. a factor of 7.5) in the intrinsic luminosity is not seen in the data. Two scenarios are proposed: either the colliding winds emission is unexpectedly weak such that intrinsic shocks in the winds dominate the emission, or, alternatively, that the emission observed *is* colliding winds emission but in a more complex form than we would naively expect. Complex hydrodynamical models are then analyzed. Despite strongly phase-variable emission from the models, *both* were consistent with the observations. We find that if the mass-loss rates of the stars are low then intrinsic wind shocks could dominate the emission. However, when we assume higher mass-loss rates of the stars, we find that the observed emission could also be consistent with a purely colliding winds origin. A summary of the strengths and weaknesses of each interpretation is presented. To distinguish between the different models X-ray observations with improved phase coverage will be necessary.

Key words: stars: individual: Iota Orionis (HD 37043) – stars: early-type – binaries: general – X-rays: stars

1 INTRODUCTION

The Orion OB1 stellar association is one of the brightest and richest concentrations of early-type stars in the vicinity of the Sun (Warren & Hesser 1977). It contains large num-

* Chargé de Recherches FNRS, Belgium

bers of young O- and B-type stars, and this, combined with its position well below the galactic plane ($\langle b \rangle = -16^\circ$) with subsequent low foreground absorption, makes it an optimal object to study. The OB1 association is also famous for an exceptionally dense concentration of stars known as the Trapezium cluster, located near θ^1 Ori. The stellar density of the Trapezium cluster has been estimated by several authors in recent years and its central region is now thought to exceed $\sim 4 \times 10^4$ stars pc^{-3} (McCaughrean & Stauffer 1994), making it one of the densest young clusters currently known.

Iota Orionis (HR 1889; HD 37043) is a well known highly eccentric ($e = 0.764$) early-type binary system (O9 III + B1 III, $P = 29.13376$ d) located in the C4 subgroup of the Orion OB1 association, approximately 30 arcminutes South of the Trapezium cluster. In the last decade Iota Orionis has drawn attention for the possibility of an enhanced, focused wind between the two stars during the relatively close periastron encounter (Stevens 1988; Gies, Wiggs & Bagnuolo 1993; Gies et al. 1996). Although data consistent with this effect was presented (residual blue-shifted emission in $\text{H}\alpha$ that accelerates from about -100 km s^{-1} to -180 km s^{-1}), previous evidence was inconclusive, and the possibility of a random fluctuation of the primary's wind was not ruled out by Gies et al. (1996). These authors also found no evidence of any systematic profile deviations that are associated with non-radial pulsations. The latest optical monitoring (Marchenko et al. 2000), again obtained data consistent with a proximity effect.

Iota Orionis is perhaps even more interesting for the possible existence of a strong colliding winds interaction region between the two stars, which should be most clearly recognized at X-ray wavelengths. As demonstrated by Corcoran (1996), perhaps the best direct test for the importance of colliding winds emission is to look for the expected variation with orbital phase. X-ray data can also be used to extract information on the characteristics of this region (e.g. geometry, size, temperature distribution), which can in turn constrain various stellar parameters including mass-loss rates. This possibility has already been explored for the Wolf-Rayet (WR) binary γ^2 Velorum (Stevens et al. 1996). Furthermore, a direct comparison of the recently presented sudden radiative braking theory of Gayley et al. (1997) with observed X-ray fluxes has not yet been made. For this goal, Iota Orionis has the dual advantage of a high X-ray flux (partially due to its relative proximity, $D \sim 450$ pc) and a highly eccentric orbit (the varying distance between the stars should act as a 'probe' for the strength of the radiative braking effect). Iota Orionis is additionally intriguing for its apparent lack of X-ray variability (see Section 2) whilst colliding wind theory predicts a strongly varying X-ray flux with orbital phase.

In this paper we present the analysis and interpretation of two *ASCA* observations of Iota Orionis proposed by the *XMEGA* group, as well as a reanalysis of some archival *ROSAT* data. These are the first detailed *ASCA* observations centered on this object, although *ASCA* has previously observed the nearby O-stars δ Ori and λ Ori (Corcoran et al. 1994) and surveyed the Orion Nebula (Yamauchi et al. 1996). *ASCA* observations of WR+O binaries (e.g. γ^2 Velorum - Stevens et al. 1996; WR 140 - Koyama et al. 1994) have provided crucial information of colliding stel-

lar winds in these systems. The new *ASCA* observations of Iota Orionis enable us to perform a detailed study of the X-ray emission in this system. The periastron observation covered ~ 65 ksec and includes primary minimum ($\phi = -0.009$), periastron passage ($\phi = 0.0$), and quadrature ($\phi = 0.014$), and allows an unprecedented look at interacting winds in an eccentric binary system over a range of different orientations. The apastron observation covered ~ 25 ksec and allows us to compare the X-ray properties at the maximum orbital separation. Thus these two new observations offer the additional benefit of improving the poor phase sampling of this object.

The new *ASCA* observations were coordinated with an extensive set of ground based optical observations reported in Marchenko et al. (2000). In this work, the spectra of the components were successfully separated, allowing the refinement of the orbital elements (including the restriction of the orbital inclination to $50^\circ \lesssim i \lesssim 70^\circ$) and confirmation of the rapid apsidal motion. Strong tidal interactions between the components during periastron passage and phase-locked variability of the secondary's spectrum were also seen. However, no unambiguous signs of the bow shock crashing onto the surface of the secondary were found. These results are extremely relevant to the interpretation of the *ASCA* X-ray data.

This paper is organized as follows: in Section 2 we briefly discuss previous X-ray observations of Iota Orionis; in Section 3 we present our analysis of the new *ASCA* datasets and reexamine archival *ROSAT* data. In Section 4 we examine possible interpretations of the data. Comparisons with other colliding wind systems are made in Section 5, and in Section 6 we summarize and conclude.

2 PREVIOUS X-RAY OBSERVATIONS OF IOTA ORIONIS

On account of its high X-ray flux, Iota Orionis has been observed on several occasions. X-ray emission from Iota Orionis was reported by Long & White (1980) in an analysis of *Einstein* Imaging Proportional Counter (IPC) data, and a count rate of 0.289 ± 0.007 cts/s in the 0.15–4.5 keV band was obtained. The spectral resolution ($E/\Delta E$) of the IPC was only 1–2, so only the crudest spectral information could be obtained, although it was observed that the spectrum was soft, peaking below 1 keV. The authors noted that qualitatively good fits could be obtained with a variety of spectral models leading to an uncertainty of a factor of 2 in their quoted luminosity of $2.3 \times 10^{32} \text{ erg s}^{-1}$ (0.15–4.5 keV).

Since this observation the X-ray properties of Iota Orionis have been studied on numerous occasions (Snow, Cash & Grady 1981; Collura et al. 1989; Chlebowski, Harnden & Sciortino 1989; Waldron 1991; Gagné & Caillault 1994; Geier, Wendker & Wisotzki 1995; Berghöfer & Schmitt 1995a; Kudritzki et al. 1996; Feldmeier et al. 1997a). Due to the different X-ray satellites, data-analysis techniques, and orbital phases, meaningful comparisons between the datasets are difficult, and we simply refer the reader to the above mentioned papers. We note, however, the results of previous X-ray variability studies of Iota Orionis, performed by Snow et al. (1981) and Collura et al. (1989) on *Einstein* data, and by Berghöfer & Schmitt (1995a) on *ROSAT* data.

Snow et al. found that the count rates from 3 IPC observations were twice as high as the Long & White observation, leading to the simple interpretation that the X-ray emission from Iota Orionis could vary by up to a factor of two (with a statistical significance of 3σ), though it was noted that at the time of the observations there were problems with the instrumental gain shifts of the IPC. Collura et al. (1989) reexamined the issue of variability with a more rigorous method and found that they could only place upper limits of 12% on the amplitude of variability over timescales ranging from 200 s up to the duration of each observational interval. In contrast to the findings of Snow et al. (1981) no evidence of long-term variability between observations was detected. Finally Berghöfer & Schmitt (1995a) found an essentially flat lightcurve from *ROSAT* observations, consistent with the previous findings of Collura et al. (1989), although again the phase-sampling was rather poor. The lack of dramatic variability in these previous studies could be a result of poor phase sampling, and/or the soft response of the instruments (assuming that X-rays from the wind collision are harder than those intrinsically emitted from the individual winds). Our *ASCA* observations were specifically designed to address this by i) sampling at phases where the variation should be maximized; and ii) by leveraging the extended bandpass of *ASCA* to measure the hard flux.

Table 1 summarizes the *Einstein* IPC observations and the rather confusing situation with regard to whether and at what level there is any variability (note that it is *not* meant to imply that there *is* any real source variability). It also emphasizes the poor phase sampling and serves as a useful highlight as to one of the reasons why the latest *ASCA* data presented in this paper were obtained. In column 3 we list the orbital phase at the time of observation, calculated from the ephemeris

$$HJD(\text{periastron}) = 2451121.658 + 29.13376E$$

derived from the latest optical monitoring of this system (Marchenko et al. 2000). As a result of the large number of orbits that have elapsed the listed phases are only approximate and do not account for the apsidal motion detected in Iota Orionis (Stickland et al. 1987, Marchenko et al. 2000). We also draw attention to the different count rates obtained by different authors when analysing the same datasets, and the relatively constant count rates obtained from different datasets by the same authors.

A further *ROSAT* analysis of Iota Orionis was published by Geier et al. (1995), who obtained a position-sensitive proportional counter (PSPC) observation centered on the Trapezium Cluster. This discovered that most of the X-ray emission from the region originated from discrete sources, in contrast to the previous *Einstein* data where the sources were spatially unresolved. Nearly all of the 171 X-ray sources were identified with pre-main sequence stars in subgroups Ic and Id of the Orion OB1 association. The 4 pointings made from March 14-18 1991, together gave a total effective exposure time of 9685 s. However, Iota Orionis was significantly off-axis in all of these pointings. Assuming a Raymond & Smith (1977) thermal plasma spectral model, a single-temperature fit gave $kT = 0.22$ keV and $N_H = 10^{20} \text{ cm}^{-2}$, whilst a two-temperature fit with a single absorption column gave $kT_1 = 0.12$ keV, $kT_2 = 0.82$ keV, and $N_H = 3 \times 10^{20} \text{ cm}^{-2}$.

Table 1. *Einstein* IPC observations of Iota Orionis.

Sequence number	Date of obs.	Phase ϕ	IPC counts/s		
			(LW80)	(SCG81)	(C89)
3842	23/9/79	0.34	0.289		
11263	03/3/80	0.90		0.609	
5095	05/3/80	0.97		0.585	0.417
5096	23/3/80	0.59		0.607	0.413
10413	16/2/81	0.92			0.367

Notes. The count rates listed were obtained from the following papers: LW80 - Long & White (1980); SCG81 - Snow, Cash & Grady (1981); C89 - Collura et al. (1989).

Two analyses of *ROSAT* PSPC spectra which ignored the binary nature of Iota Orionis have recently been published by Kudritzki et al. (1996) and Feldmeier et al. (1997a). The X-rays were assumed to originate from cooling zones behind shock fronts. These are a natural development of the intrinsically unstable radiative driving of hot-star winds (see e.g. Owocki, Castor & Rybicki 1988). Although the authors stated that good fits were obtained, no formal indication of their goodness was given. Because binarity may significantly affect the X-ray emission, we use this as the basis of our interpretation of the data. This approach complements these alternative single-star interpretations.

3 THE X-RAY DATA ANALYSIS

Despite previous attempts to characterize the X-ray properties of Iota Orionis, our understanding remains poor. For instance, from the previous *Einstein* and *ROSAT* data it looks like a typical O-star. However, on account of its stellar and binary properties, Iota Orionis should reveal a clear X-ray signature of colliding stellar winds which one would expect to show dramatic orbital variability as the separation between the stars changes. *ASCA* should be well suited for the study of this emission on account of its high spectral resolution and greater bandpass. In this section we report on the analysis performed on the two new phase-constrained *ASCA* datasets. This is followed by a reanalysis of two archival *ROSAT* datasets, and a comparison with results obtained from colliding wind models.

3.1 The *ASCA* analysis

3.1.1 Data reduction

Iota Orionis was twice observed with *ASCA* during 1997[†]. An observation on 21 September 1997 was timed to coincide with periastron passage, whilst the 6 October observation was timed to coincide with apastron passage. The event files from each instrument were screened using the FTOOL ASCASCREEN. For the standard SIS analysis the BRIGHT datamode was processed using medium and high bit rate

[†] Details of the *ASCA* satellite may be found in Tanaka, Inoue & Holt (1994).

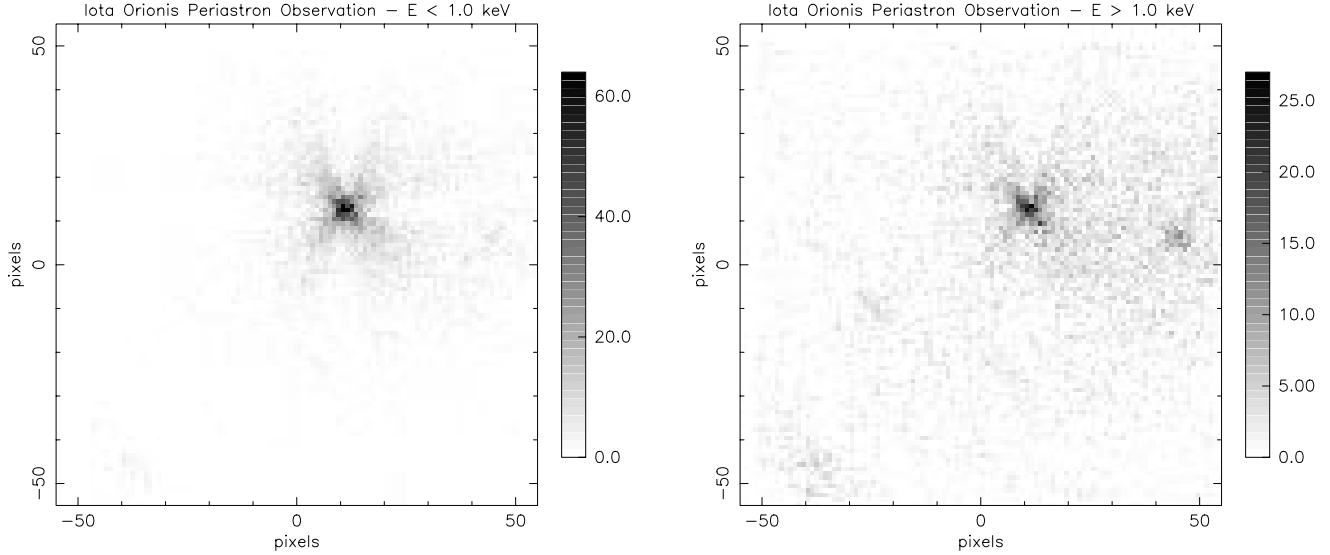


Figure 1. Screened images from the SIS0 periastron data at energies below 1.0 keV (left) and above 1.0 keV (right). The serendipitous source is noticeably brighter in the image on the right, which tells us that its spectrum is relatively harder than Iota Orionis. The left image clearly shows the characteristic ‘Maltese Cross’ of the XRT PSF.

Table 2. Effective exposure times and number of counts (background corrected) for each of the four instruments onboard *ASCA* during the periastron and apastron pointings. The percentage of counts in the source region due to background varied between 20–25 per cent for the periastron pointing and 15–23 per cent for the apastron pointing. The orbital phase spanning each observation is also listed in column 1.

Observation (Phase, ϕ)	Inst.	Exp. (s)	Cts in source region	Ct rate (s^{-1}) in source region
Periastron 0.9905–1.068	SIS0	65672	12543	0.191
	SIS1	66545	9729	0.146
	GIS2	72288	4301	0.060
	GIS3	72336	5085	0.070
Apastron 1.502 – 1.529	SIS0	23934	4856	0.203
	SIS1	23798	3225	0.136
	GIS2	24496	1416	0.058
	GIS3	24496	1814	0.074

data. Hot and flickering pixels were removed and the standard screening criteria applied.

The four X-ray telescopes (XRTs) onboard *ASCA* each have spatial resolutions of 2.9 arcmin half power diameter. In spite of the broad point-spread function (PSF), the jittering of the spacecraft can appear on arcminute scales. To avoid inaccurate flux determinations and spurious variability in the light curves, the radius of the source region should normally be no smaller than 3 arcmin (*ASCA* Data Reduction Guide). For most cases the recommended region filter radius for bright sources in the SIS is 4 arcmin. Because of

concerns of contamination from nearby sources, our standard analysis adopted a source radius of 3 arcmin.

The estimation of the X-ray background initially proved somewhat troublesome. The presence of a nearby source forced a thin annulus, creating a large variance on the background spectrum, which invariably still contained contaminating counts. The available blank sky backgrounds were also found to be unsatisfactory. After much consideration, the background was estimated from the entire CCD excluding the source region and other areas of high count rate. This method produced a large number of background counts, reducing the uncertainty in its spectral shape, and resulting in a spectral distribution for the source which was better constrained.

For the GIS analysis, the standard rejection criteria for the particle background were used together with the rise time rejection procedure. Unlike the SIS, the intrinsic PSF’s of the GIS are not negligible compared to the XRT’s and a source region filter of 4 arcmin radius was used. The serendipitous source detected by the SIS instruments was not spatially resolved by the GIS instruments and hence the source spectra extracted from the latter contain contaminating counts from this object.

Two methods of background subtraction for the GIS instruments are commonly used. Either one can use blanksky images with the same region filter as used for the source extraction, or one can choose a source-free area on the detector at approximately the same off-axis angle as the source. In our analysis the second method was favoured due to the following reasons:

- (i) The cut-off-rigidity (COR) time-dependence can be correctly taken into account.
- (ii) The blanksky background files were taken during the

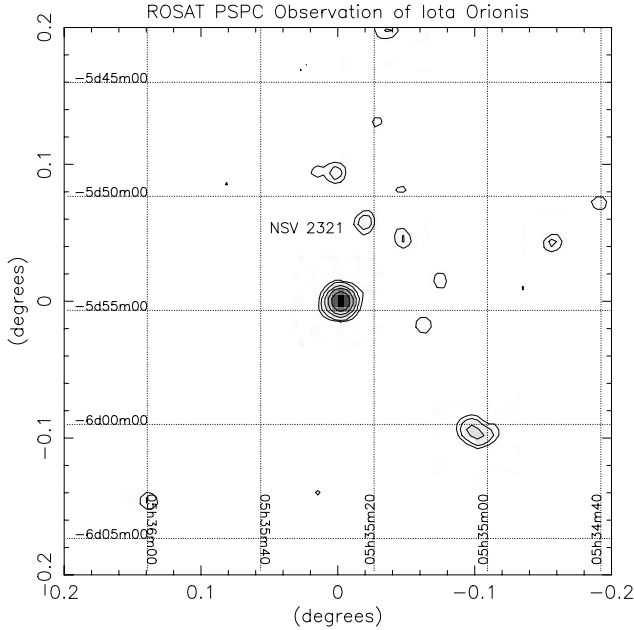


Figure 2. *ROSAT* PSPC image of the Iota Orionis field. This image number is rf200700n00, and clearly shows the X-ray sources near Iota Orionis, which is the brightest source at the centre of the field. The serendipitous *ASCA* source is labelled. Contour levels are 1, 2, 5, 10, 20 and 50 counts. Epoch 2000.0 coordinates are shown.

early stages of the *ASCA* mission, and do not include the secular increase of the GIS internal background.

- (iii) The blanksky background files were also taken from high Galactic latitude observations, and hence possible diffuse X-ray emission near Iota Orionis cannot be taken into account.

Despite these reasons, the blanksky method of background subtraction was also tested and in contrast to the SIS analysis both methods produced spectral fit results which agreed within their uncertainties. However, all subsequent work including the results reported in this paper used a background extracted from the same field as the source.

The effective exposure times and count rates for the various instruments during the periastron and apastron pointings are detailed in Table 2. The numbers in columns 4 and 5 refer only to the specific source regions extracted.

In Fig. 1 we show the SIS0 field from the periastron observation for two different energy bands. In addition to Iota Orionis, a serendipitous source is clearly visible to the right, being most noticeable in the harder image. A *ROSAT* PSPC image of Iota Orionis is shown in Fig. 2, and demonstrates more clearly the crowding of sources in this region of the sky. The serendipitous source in Fig. 1 is tentatively identified as NSV 2321, an early G-type star (optical coords: RA(2000.0) = 05^h 35^m 22^s, Dec.(2000.0) = −05° 54′ 35″). As already noted, this source complicates the analysis, of which more details are given in Section 3.1.4.

3.1.2 The X-ray lightcurves

Lightcurves from all 4 instruments were extracted for each of the two observations and analysed with the XRONOS package. A subset of these is shown in Fig. 3. Somewhat surprisingly the lightcurves were found to be remarkably constant. For the periastron SIS0 observation, a fit assuming the background-subtracted source was constant gave $\chi^2_\nu = 0.85$. For the apastron observation a corresponding analysis gave $\chi^2_\nu = 0.75$. If the majority of the X-ray emission was from the wind collision region, one would expect significant variation given the highly eccentric nature of the system. There is also little difference between the count rates of the periastron and apastron observations.

However, close to periastron passage (corresponding to 2.38×10^4 s after the start of the observation) there does seem to be a small transient spike in both the SIS0 (see Fig. 3) and GIS2/3 count rates (although nothing appears in the SIS1 lightcurve). This ‘flare’ is of relatively low significance, and could be entirely instrument related as it occurs just before an interval of bad data. Supporting evidence for this comes from Moreno & Koenigsberger (1999) who have recently investigated the effect of tidal interactions between the stars around periastron passage. They found that if the radius of the primary is smaller than 15 R_\odot , the enhancement in the mass-loss rate at periastron, and therefore the effect on the colliding winds emission, should not be significant. However, the phasing of the X-ray flare is almost perfect with a similar event seen in the optical (Marchenko et al. 2000). To examine whether the flare possibly occurred in the background a cross-correlation analysis was performed. No significant correlation was found between the source and background lightcurves, whilst a strong correlation clearly occurred between the unsubtracted and subtracted source lightcurves. We conclude, therefore, that it is unlikely that this ‘flare’ occurs in the background data.

3.1.3 The X-ray spectra

Using the XSPEC package, source X-ray spectra were extracted from each dataset, re-binned to have a minimum of 10 counts per bin (as required for χ^2 -fitting), and fitted with both single and two-temperature Raymond-Smith (RS) spectral models. We emphasize at this point that this simple analysis is an effort to *characterize* i) the overall shape of the spectrum and its temperature distribution, ii) the amount of variability in the spectral parameters, and iii) the discrepancies between theoretical colliding stellar wind spectra and the observed data (see Section 4.2). It is not meant to imply that in the two-temperature fits the emission physically occurs from two distinct regions at separate temperatures, and is simply in keeping with X-ray analysis techniques commonly used today. The upper panel of Fig. 4 shows a two-temperature RS model with one absorption component that has been simultaneously fitted to the SIS0 and SIS1 periastron datasets, whilst the lower panel shows the corresponding fit to the GIS2 and GIS3 periastron datasets. We include data down to ~ 0.5 keV for the SIS instruments (important for measuring changes in N_H , although see Section 3.1.4) and to ~ 0.8 keV for the GIS instruments (where the effective area is roughly 10 per cent of the maximum effective area for this instrument, thus en-

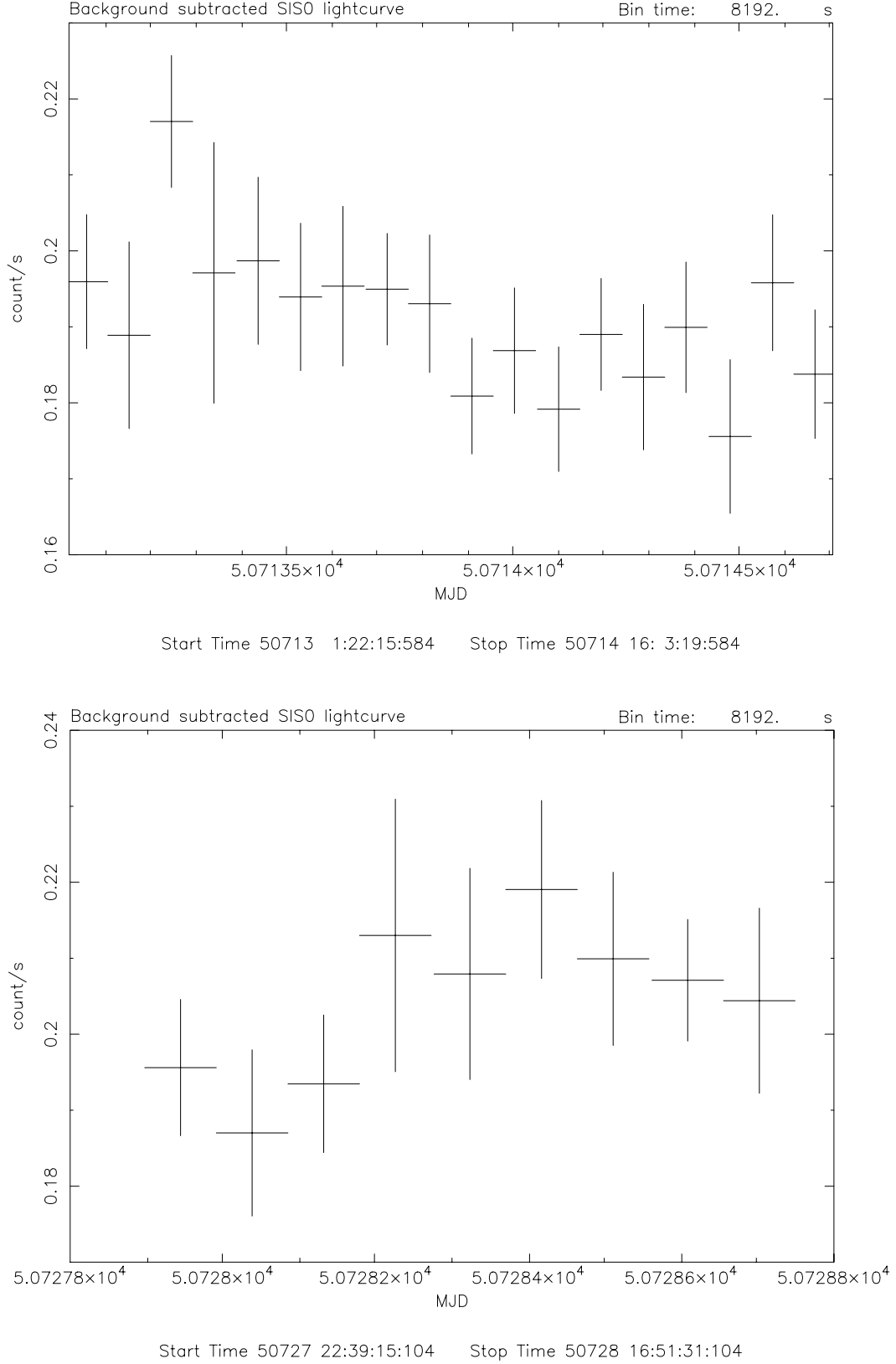


Figure 3. Background subtracted lightcurves from the SIS0 detector for the periastron (top) and apastron (bottom) observations. They are remarkably constant considering the anticipated wind interaction. However, an emission ‘spike’ is clearly seen in the periastron lightcurve, which occurs just before the point of closest approach of the stars (MJD = 50713.28536). It is not seen in the SIS1 data, though, and we note that it occurs just before a period of bad data, and therefore could be entirely instrumental.

abling us to extract maximum information about the emission below 1.0 keV).

Some line emission is clearly seen, in particular at ~ 1.85 keV and at ~ 2.30 keV, of which the former is most probably from SiXIII. Numerous spectral models were fitted to the data on both an instrument by instrument basis and to various combinations of the four instruments including all four instruments together. First we attempted single temperature solar abundance fits. Only the fit to the combined GIS2 and GIS3 apastron data was acceptable: $N_H = 2.71 \pm 0.63 \times 10^{21} \text{ cm}^{-2}$, $kT = 0.61 \pm 0.06$ keV, $EM = 7.7 \pm 1.7 \times 10^{54} \text{ cm}^{-3}$, $\chi^2_\nu = 0.92$. Fits using non-solar abundances were not significantly improved, although the addition of a second independent plasma component did result in much better fits and we report some results in Table 3. Immediately obvious is that the fits to the periastron and apastron SIS data are very similar, both in terms of the spectral parameters and the resulting luminosities. Clearly there is not the order of magnitude variation which we expected in the intrinsic luminosity. This is also true for the corresponding fits to the GIS data. Thus it appears at first glance that any variability is small. This has implications for a colliding winds interpretation of the data, although at this stage we do not rule this model out. Other general comments which we can make on the spectral fits are:

- (i) The SIS datasets return much higher values of N_H and much lower values of the characteristic temperature, kT , than the GIS datasets.
- (ii) Both the SIS and GIS fits return absorbing columns which are greater than the estimated interstellar column ($2.0 \times 10^{20} \text{ cm}^{-2}$; Shull & Van Steenberg 1985, and Savage et al. 1977) arguing for the presence of substantial circumstellar absorption consistent with strong stellar winds.
- (iii) Due to the larger variance on the GIS data, the GIS fit results are statistically acceptable, whereas those to the SIS data are not.
- (iv) If the global abundance is allowed to vary during the fitting process, the general trend in the subsequent fit results is that the characteristic temperature increases, the absorbing column decreases, the normalization increases, and the abundance fits at 0.05–0.2 solar. The resulting χ^2_ν is basically unchanged. These fit results bear all the hallmarks of the problems mentioned by Strickland & Stevens (1998) and we question their accuracy.
- (v) The metallicities generally fit closer to solar values if a two-temperature RS model is used.
- (vi) If a simultaneous SIS and GIS fit is made, the returned temperatures are similar to those from the SIS dataset alone. This is perhaps not so surprising, however, given that the variance on the GIS data is much larger than the SIS, and therefore that the SIS data has a much larger influence in constraining the fit.

Two-temperature RS models with separate absorbing columns to each component were also fitted, as were two temperature spectral models with neutral absorption fixed at the ISM value and an additional photoionized component. However, both failed to significantly improve the fitting and we do not comment on these further.

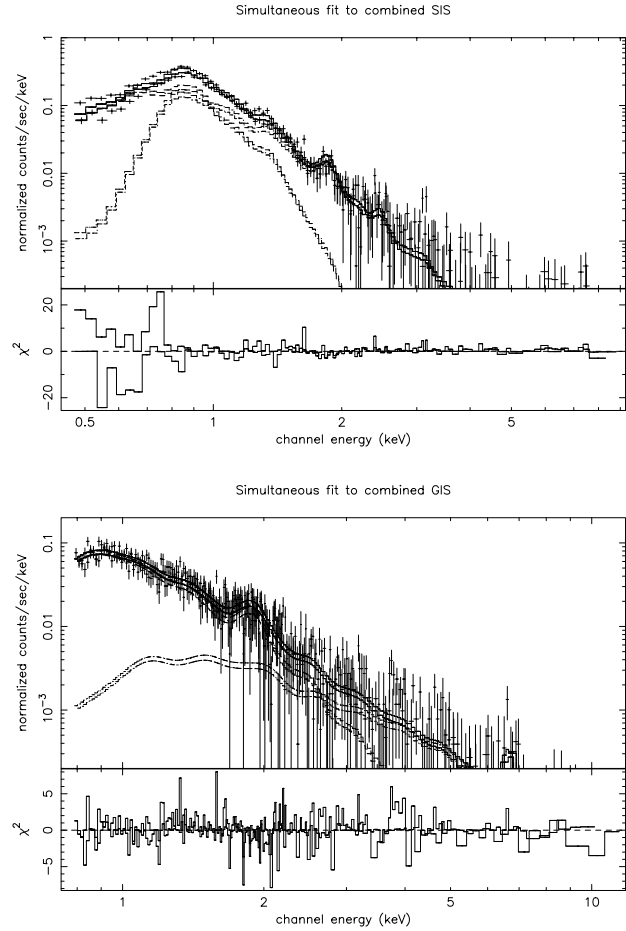


Figure 4. Two-temperature Raymond-Smith spectral model fits to the combined SIS0 and SIS1 data (upper panel) and the combined GIS2 and GIS3 data (lower panel) from the entire periastron observation. Both spectral components and the combined model are shown, together with the data. A minimum of 10 counts is in each data bin.

3.1.4 Problems with the analysis

Although the differences between the individual SIS0 and SIS1 datasets, and between the GIS2 and GIS3 datasets are within the fit uncertainties, there is a large discrepancy between the fit results made to the SIS datasets on the one hand and the GIS datasets on the other. Models which fit the GIS do not fit the SIS, and vice-versa. Whilst we can already state with some confidence that the X-ray emission is not strongly variable, the above is obviously a large cause for concern which we should still explore. For instance, if we ignore the lack of variability for a moment and assume that a colliding winds scenario is the correct model, then the fitted temperatures should provide some information on the pre-shock velocities of the two winds, and whether these vary as a function of orbital phase. Hence for this reason we wish to determine which of the SIS or GIS temperatures is most accurate.

First the fit-statistic parameter space was investigated for false or unphysical minima. This is shown in Figure 5 for a single-temperature RS model fitted to the SIS0 and GIS2 periastron data. It is clear that there are no additional

Table 3. Two-temperature spectral fitting results. Fits made to the combined SIS0 and SIS1 datasets and the combined GIS2 and GIS3 datasets are shown, as well as that to an archive *ROSAT* dataset (see Table 4). The estimated ISM column is $2.0 \times 10^{20} \text{ cm}^{-2}$. The emission measure and luminosities (0.5 – 2.5 keV) were calculated assuming a distance of 450 pc. The emission measure to the soft component of the rf200700n00 fit could not be constrained and led to unrealistic luminosities. Consequently we do not include it here. Many other spectral models were also examined (see main text) but for conciseness and simplicity we do not report them here.

Data	N_H (10^{21} cm^{-2})	kT_1 (keV)	kT_2 (keV)	EM_1 (10^{54} cm^{-3})	EM_2 (10^{54} cm^{-3})	χ^2_ν (DOF)	$L_x(\text{int})$ ($10^{32} \text{ erg s}^{-1}$)	$L_x(\text{abs})$ ($10^{32} \text{ erg s}^{-1}$)
Periastron SIS	$5.07^{+0.28}_{-0.28}$	$0.14^{+0.01}_{-0.01}$	$0.61^{+0.02}_{-0.02}$	260^{+61}_{-61}	$4.6^{+0.5}_{-0.5}$	2.06 (225)	20.17	1.04
Apastron SIS	$3.90^{+0.53}_{-0.53}$	$0.15^{+0.01}_{-0.01}$	$0.61^{+0.03}_{-0.03}$	94^{+47}_{-47}	$4.1^{+0.7}_{-0.7}$	2.06 (143)	8.99	1.00
Periastron GIS	$1.97^{+0.55}_{-0.76}$	$0.61^{+0.05}_{-0.04}$	$3.12^{+2.31}_{-0.92}$	$6.06^{+0.97}_{-1.21}$	$0.94^{+0.36}_{-0.34}$	1.08 (381)	2.01	1.08
Apastron GIS	$4.73^{+1.43}_{-1.46}$	$0.25^{+0.10}_{-0.07}$	$2.15^{+0.70}_{-0.58}$	68^{+266}_{-46}	$2.0^{+0.96}_{-0.65}$	0.77 (210)	12.3	1.46
rp200700n00	$0.28^{+0.42}_{-0.15}$	$0.11^{+0.03}_{-0.05}$	$0.70^{+0.13}_{-0.14}$	$26.7^{+806}_{-14.6}$	$3.63^{+0.73}_{-0.73}$	0.61 (11)	1.85	1.60

minima between the two shown, and the SIS0 minimum in particular is very compact. However, at very high confidence levels there is a noticeable extension of the GIS2 confidence region towards the SIS0 minimum. Despite this the results seem to be totally incompatible with each other. Other possible explanations for the observed discrepancy are offered below:

Degradation of the SIS instruments

The HEASARC website (<http://heasarc.gsfc.nasa.gov/docs/asca/watchout.html>) reports that there is clear evidence for a substantial divergence of the SIS0 and SIS1 detectors since late 1994, with even earlier divergence between the SIS and GIS data. It is also noted that both the SIS0 and SIS1 efficiencies below 1 keV have been steadily decreasing over time, which at 0.6 keV can be as much as 20 per cent for data taken in 1998. The loss in low-energy efficiency manifests itself as a higher inferred column density, introducing an additional N_H uncertainty of a few times 10^{20} cm^{-2} . This is consistent with our results where the SIS detectors return higher values of N_H than the GIS (see Table 3), although we note that the difference in our fits can often be much larger. An increasing divergence of the SIS and GIS spectra in the energy range below 1 keV has also been noted by Hwang et al. (1999). As also noted on the HEASARC website a related problem is that the released blank-sky data cannot be used for background-subtraction for later SIS data since the blank-sky data was taken early on in the ASCA mission. This is also consistent with the problems mentioned in Section 3.1.1 in obtaining good fits when using this method of background subtraction. Whilst these problems offer a convincing explanation for the discrepancies in our fits, we should investigate further before dismissing the SIS results in favour of the GIS results.

Contamination of the GIS data

The serendipitous source (hereafter assumed to be NSV 2321) seen in the SIS field is included in the GIS spectrum due to the larger PSF of the latter. In section 3.1.1 it was remarked that NSV 2321 was intrinsically harder than the Iota Orionis spectrum (see also Fig. 1). To examine the effect of NSV 2321 on the fit results, a 1.06 arcmin radius circular region centred on NSV 2321 was extracted from the SIS0 periastron data. Although the quality of the spectrum

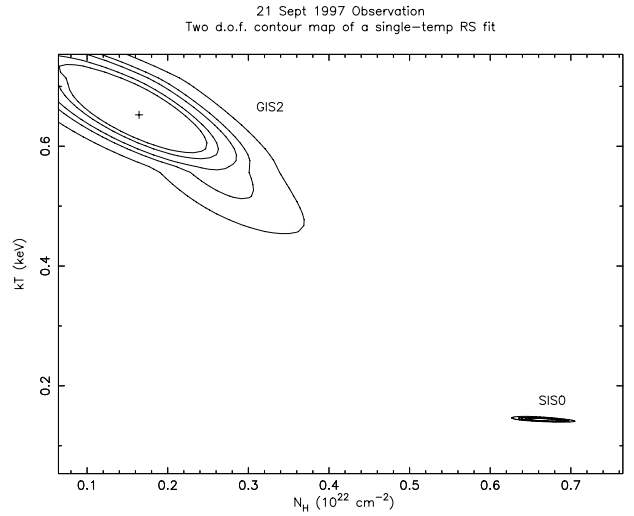


Figure 5. This figure shows the fit-statistic parameter space for a single-temp RS model fitted separately to the SIS0 and the GIS2 periastron data. The contour levels plotted are the 90.0, 95.4, 99.0, 99.73 and 99.99 per cent confidence regions.

was poor the fit results confirm that it is a harder source than Iota Orionis, which is consistent with the GIS fits having higher characteristic temperatures than the SIS fits.

Intrinsic bias

Another possibility for the differences between the SIS and GIS results may lie in the fact that compared with the SIS instruments, the GIS instruments are more sensitive at higher X-ray energies. This may result in fits to the GIS data intrinsically favouring higher characteristic temperatures. To investigate this we performed fits to a GIS spectrum whilst ignoring the emission above selectively reduced energy thresholds. The results are shown in Fig. 6 where a clear bifurcation in the fit results can be seen. As more high energy X-rays are ignored, the fit jumps from a high temperature and low column to a low temperature and high column which is much more compatible with the SIS results. After discovering this behaviour the SIS0 data was analysed in a similar manner but reversing the process and selectively ignoring X-rays below a certain threshold. Again, a bifurcation

Table 4. Effective exposure times and background subtracted count rate and number of counts in the source region for the two *ROSAT* PSPC observations examined. The ‘rf’ dataset was Boron filtered which blocks X-ray photons with energies between 0.188-0.28 keV.

Observation	Phase	Exp. (s)	Cts	Ct rate (s ⁻¹)
rp200700n00	0.1697 - 0.1841	746	1153	1.545
rf200700n00	0.1841 - 0.1846	1305	489	0.374

develops, this time towards the original GIS results. This is strong evidence that there is either an intrinsic bias in the instrument calibrations (either present in the original calibrations, or a result of the instrument responses changing with time), or that the fitting process itself is flawed i.e. that if we fit a single-temperature spectral model to an inherently multi-temperature source, the SIS fit will have a lower characteristic temperature than the GIS fit. Therefore are our fits simply telling us that the source is multi-temperature? In this case both the SIS and GIS results would be equally ‘incorrect’.

3.2 Re-analysis of archival *ROSAT* data

A search of the *ROSAT* public archive for observations of Iota Orionis yielded a total of 3 PSPC pointed observations. Two were back-to-back exposures with Iota Orionis on axis, of which one used the Boron filter. The other had Iota Orionis far off-axis (outside of the rigid circle of the window support structure). An advantage of the *ROSAT* observations is that Iota Orionis is resolved from nearby X-ray sources. NSV 2321 is spatially resolved from Iota Orionis in two of the three PSPC pointings, and we have reanalysed both of these. Details of each observation are listed in Table 4.

A single temperature RS model could not reproduce the observed data for either observation. However, fits with two characteristic temperatures showed significant improvement and acceptable values of χ^2_ν were obtained. Unfortunately an unrealistically soft component was obtained from the Boron filtered dataset which led to an artificially high luminosity. The fit to the other dataset is detailed in Fig. 7 and Table 3. We note that if separate columns are fitted to each component the column to the harder component is much higher than that to the softer component and the estimated ISM value.

Our results can be compared to the analysis by Geier et al. (1995), who obtained characteristic temperatures of 0.12 and 0.82 keV from a two-temperature RS fit made to the rp200151n00 dataset. As already noted, Iota Orionis was substantially off-axis in this pointing and the nearby sources seen in Fig. 2 were unresolved. This may account for the slightly higher temperatures that they obtained.

We can also compare our *ROSAT* results to the *ASCA* results obtained in the previous section. In so doing we find distinct differences between the parameters fitted to the 3 individual detectors (SIS, GIS and PSPC), although roughly equivalent attenuated luminosities. In particular,

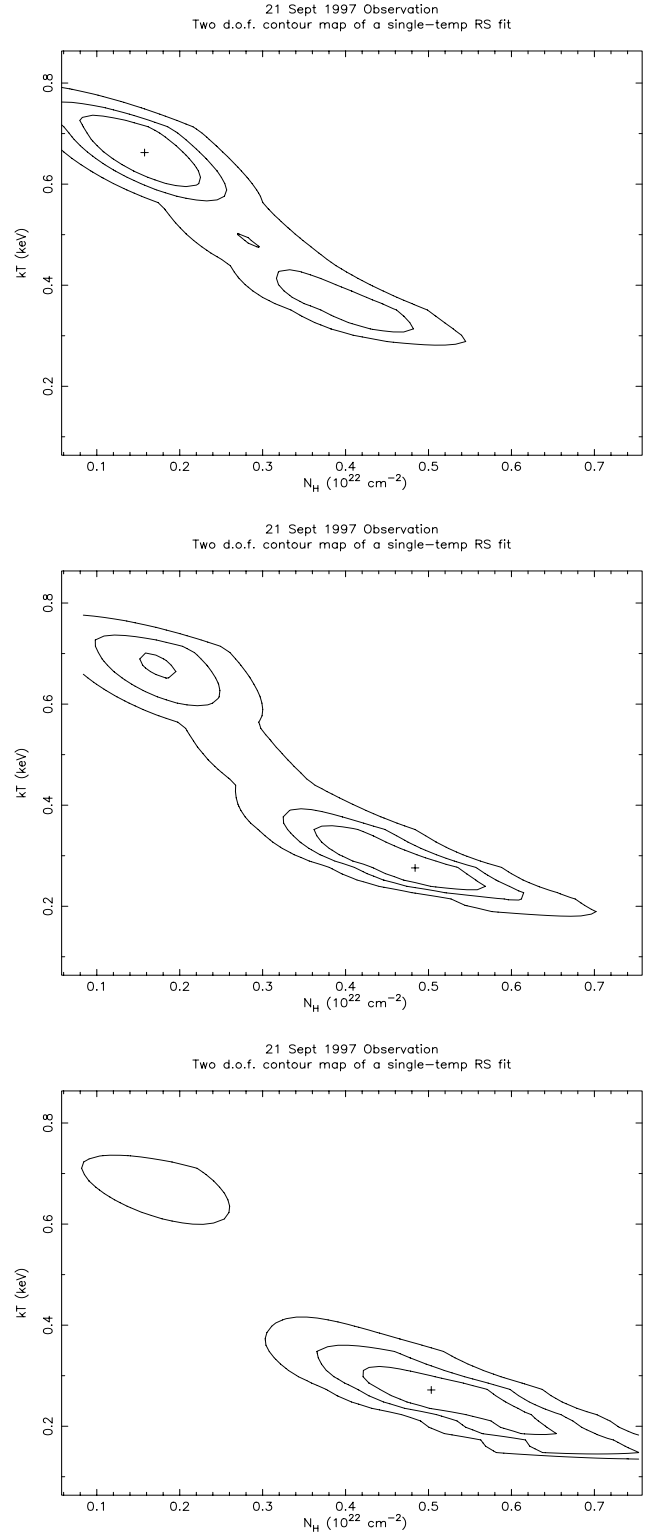


Figure 6. This figure shows the fit-statistic parameter space for a single-temp RS model fitted to a GIS2 spectrum extracted from a 2 arcmin radius circle centered on Iota Orionis. The emission above certain energy thresholds was ignored during the fit process. For the top, middle and bottom panel these were 2.0, 1.7 and 1.2 keV respectively. The contour levels plotted are the 68.3, 90.0 and 99.0% confidence regions. The change from one minimum to the other is clearly shown.

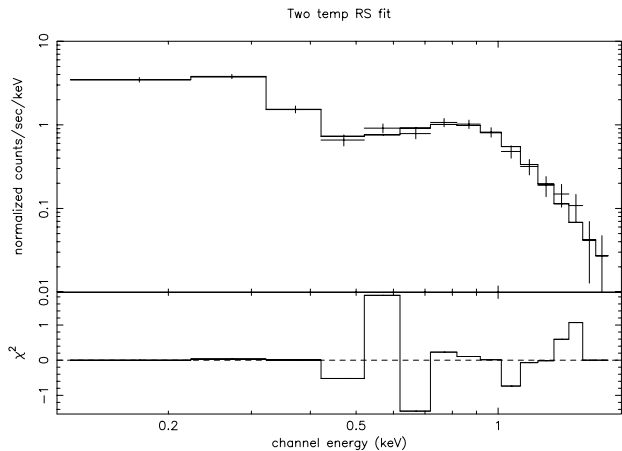


Figure 7. Two-temperature Raymond-Smith spectral model fit to the rp200700n00 *ROSAT* PSPC dataset. The large deviations between the model and the data at $E \sim 0.5$ keV may be due to uncertainties in the calibration of the PSPC detector response.

the *ROSAT* spectrum has a significantly larger flux at soft energies.

3.3 The preferred datasets

This leads us to the crucial question: which dataset do we have most confidence in? The negative points of each are:

- The SIS datasets are invariably affected by the degradation of the CCDs.
- The GIS does not have a particularly good low energy response and does not spatially resolve the close surrounding sources which contaminate the subsequent analysis.
- The PSPC has poor spectral resolution compared to the SIS and GIS.

Despite the better spectral resolution of both instruments onboard *ASCA*, it would seem (from the uncertainties mentioned in Section 3.1.4) that the *ROSAT* dataset returns the most accurate spectral fit parameters. However, the better spectral capabilities of *ASCA* convincingly demonstrates that there is no significant variation in the luminosity, spectral shape or absorption of the X-ray emission between the periastron and apastron observations.

3.4 The X-ray luminosities

The attenuated (i.e. absorbed) X-ray luminosity in the 0.5–2.5 keV band of the rp200700n00 *ROSAT* PSPC dataset (fitted by a two-temperature RS spectral model with one absorbing column) is $\sim 1.6 \times 10^{32} \text{ erg s}^{-1}$. As previously mentioned it is often not easy to compare values with those estimated in previous papers because of the different spectral models assumed, the various energy bands over which the luminosities were integrated, the different methods of background subtraction employed, and the possible contamination from nearby sources (e.g. NSV 2321). However, as reported in Section 2, Long & White (1980) estimated an attenuated luminosity of $L_x = 2.3 \times 10^{32} \text{ erg s}^{-1}$ from a single

Einstein IPC observation. Chlebowksi, Harnden & Sciortino (1989) obtained $L_x = 3.0 \times 10^{32} \text{ erg s}^{-1}$ from seven *Einstein* IPC pointings. These values are within a factor of 2 of the observed *ROSAT* 0.5–2.5 keV luminosity from the rp200700n00 dataset ($1.6 \times 10^{32} \text{ erg s}^{-1}$). This is not unexpected given the differences in the various analyses. The 0.5–10.0 keV luminosities from our analysis of the *ASCA* datasets ($\sim 1.0 \times 10^{32} \text{ erg s}^{-1}$), are also in rough agreement with the 0.5–2.5 keV *ROSAT* values, albeit slightly reduced for both the periastron and apastron observations.

Because the *ASCA* datasets have much better spectral resolution, it would be a missed opportunity if we did not take advantage of this. Thus, whilst again acknowledging that the *ASCA* results may be *systematically* incorrect, in Fig. 8 we show the intrinsic and attenuated flux *ratios* of the periastron and apastron observations. The fluxes are integrated in the energy ranges 1.0–2.0, 2.0–3.0, 3.0–4.0, 4.0–5.0, 5.0–6.0 and 6.0–7.0 keV although we note that the counts above 6.0 keV are minimal. Two-temperature RS spectral model fits were made to the combined SIS0 and SIS1 data, the combined GIS2 and GIS3 data, and all four datasets together. The top panel shows the intrinsic flux ratio, whilst the lower panel shows the attenuated flux ratio.

Immediately clear from Fig. 8 is the fact that the intrinsic luminosity from the fit of all four datasets is almost constant between periastron and apastron, and this is also basically the case for the attenuated luminosity. If the majority of the X-ray emission was due to colliding winds, one would expect the X-ray flux at periastron to be near maximum, since L_x is proportional to $1/D$. However, at energies above ~ 1 keV, the intrinsic L_x could be severely reduced around periastron as the shorter distance between the stars decreases the maximum pre-shock wind velocities. These effects are not seen.

Assuming that the bolometric luminosity of the Iota Orionis system is $L_{bol} = 2.5 \times 10^5 L_\odot$ (Stickland et al. 1987), we obtain $\log L_x/L_{bol} = -6.78$ from the *observed ROSAT* luminosity. This compares to a value of $-6.60^{+0.16}_{-0.17}$ deduced from an *Einstein* observation (Chlebowski, Harnden & Sciortino 1989). It is in even better agreement with the new results of Berghöfer et al. (1997) who obtain $\log L_x/L_{bol} = -6.81$ ($\sigma = 0.38$) for stars of luminosity classes III–V and colour index $(B - V) \lesssim -0.25$, which are appropriate for Iota Orionis. These results suggest that any emission from a colliding winds shock is at a low level (< 50 per cent of the total emission), consistent with the lack of variability between the *ASCA* pointings. We also repeat at this point the comment made by Waldron et al. (1998) on the validity of the L_x/L_{bol} relationship: that the canonical ratio ($L_x/L_{bol} \sim 10^{-7}$) should only be interpreted as an *observed* property of X-ray emission from OB stars.

4 INTERPRETATION

In the previous sections we have reported some very puzzling results. Iota Orionis was previously thought likely to have a colliding winds signature which would show significantly different characteristics between periastron and apastron, and which would act as a test-bed for the latest colliding wind theories, such as radiative braking. Although there are con-

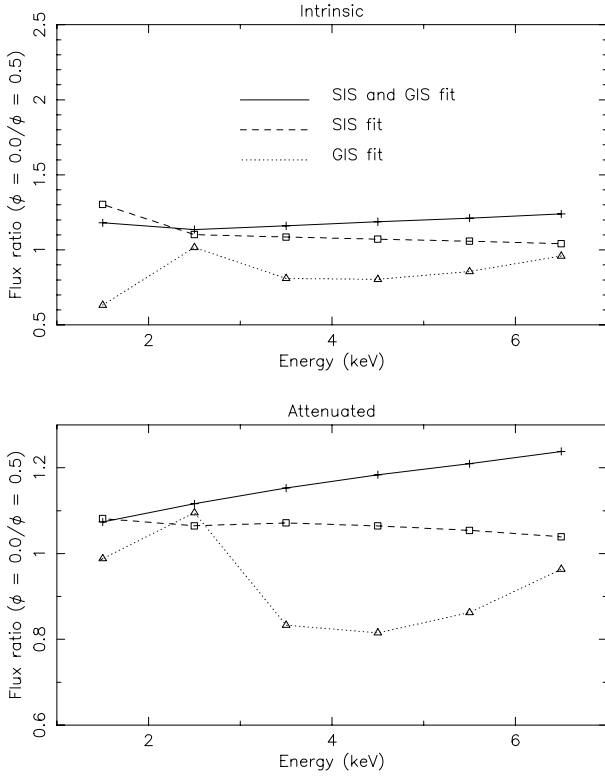


Figure 8. Ratio of the periastron and apastron intrinsic (top) and attenuated (bottom) fluxes as calculated from a two-temperature RS spectral model fitted to the *ASCA* instruments indicated. The symbols are plotted at the center of the energy band over which the fluxes were integrated (see Section 3.4).

cerns over the accuracy of the *ASCA* data and the absolute values of the fit results, it is still possible to compare relative differences between the periastron and apastron observations. However, we find that the *ASCA* X-ray lightcurves and fitted spectra show incredibly little difference between the two pointings.

The extracted spectra also have lower characteristic temperatures than originally expected, especially for the apastron observation where the primary’s wind should collide with either the secondary’s wind or its photosphere at close to its terminal velocity (see Pittard 1998).

So, the issue is why there is not an obvious colliding winds X-ray signal in Iota Orionis. Given the evidence for colliding winds in other systems it seems unlikely that there is something fundamentally wrong with the colliding winds paradigm. Two interpretations are therefore possible. One is that the majority of the observed emission is from intrinsic shocks in the winds of one or both stars (c.f. Feldmeier et al. 1997a and references therein) which dominates a weaker colliding winds signal. In this scenario the variation of the observed emission with orbital separation would be expected to be small given the large emitting volume and the lack of substantial intrinsic variability. Alternatively the emission could be from a colliding winds origin but in a more complex form than one would naively expect. In the following subsections we focus our attention on each of these in turn.

4.1 The circumstellar absorption

Before discussing the merits and faults of each of these scenarios, it is important to have a good understanding of the level and variability of the circumstellar absorption in the system. In Feldmeier et al. (1997a) a model for the wind attenuation of the primary star was derived from modelling of the UV/optical spectrum. They concluded that the wind of the primary O-star is almost transparent to X-rays. If the attenuation is indeed negligible then (since the intrinsic X-ray colliding winds luminosity is expected to change as $1/D$) we would expect to see variability in the *ASCA* data. The fact that we do not has led us to re-consider the attenuation in the system from a colliding winds perspective, and we have calculated the absorbing column to the apex of the wind collision region as a function of orbital phase. This gives us an idea of the transparency of the wind along the line of sight to the shock apex. The basic assumptions involved in the construction of this model were:

- The winds of both stars are spherically symmetric and are characterized by the velocity law

$$v(r) = v_{\infty} \left(1.0 - \frac{R_*}{r}\right)^{\beta} \quad (1)$$

where $\beta = 0.8$.

- The wind collision shock apex is determined solely by a ram-pressure momentum balance. No radiation effects such as radiative inhibition or braking are included.
- Where no ram-pressure balance exists the shock collapses onto the photosphere of the secondary and the apex is therefore located where the line of centers intersects the secondary surface.
- The shock is not skewed by orbital motion.
- The shock half-opening angle, θ , is determined from the equation

$$\theta \simeq \left(1 - \frac{\eta^{2/5}}{4}\right) \eta^{1/3} \quad (2)$$

for $10^{-4} \leq \eta \leq 1$ where

$$\eta = \frac{\dot{M}_2 v_2}{\dot{M}_1 v_1}. \quad (3)$$

v_1 and v_2 are the pre-shock velocities of the primary and secondary winds at the shock apex. This is basically the equation presented in Eichler & Usov (1993) but modified for non-terminal velocity winds.

The line of sight to Earth from the shock apex is calculated and the circumstellar absorbing column along it evaluated from knowledge of the wind density and the position of the shock cone. The ISM absorption is not added because it is constant with orbital phase and we are primarily interested in the variation (and it is also much smaller at $N_H \sim 2.0 \times 10^{20} \text{ cm}^{-2}$).

The orbit assumed for the calculation is shown in Fig. 9. It is based on the cw_1 model presented in Pittard (1998). The direction of Earth is marked, as well as the position of the secondary star relative to the primary at various phases. In Fig. 10 we show the resulting orbital variability of the circumstellar column with orbital and stellar parameters appropriate for Iota Orionis (the values used were again for model cw_1 in Pittard 1998, which for convenience we list in

Table 5. Parameters used for the hydrodynamical models cw_1 and cw_2 – see Pittard (1998) for a discussion of the observational estimates. A subscript 1 (2) indicates the value for the primary (secondary) star.

Parameter	Model cw_1	Model cw_2
$\dot{M}_1 (\text{M}_\odot \text{yr}^{-1})$	6.16×10^{-7}	3.06×10^{-7}
$\dot{M}_2 (\text{M}_\odot \text{yr}^{-1})$	1.88×10^{-8}	5.10×10^{-9}
$v_{\infty 1} (\text{km s}^{-1})$	2300	2380
$v_{\infty 2} (\text{km s}^{-1})$	2200	1990

Table 5) with a range of orbital inclinations. For $i = 90^\circ$ the numerical results were checked against an analytical form.

Unlike binaries with circular orbits, the circumstellar column as a function of phase for an inclination $i = 0^\circ$ is *not* constant, being lower at apastron than at periastron. In Fig. 10 this variation is approximately an order of magnitude. This is a direct result of the density of the primary’s wind enveloping the shock cone being higher at periastron than at apastron, which mostly reflects the combination of the change in the orbital separation and the pre-shock velocity of the primary.

At higher inclinations ($i \gtrsim 30^\circ$) the shock apex is occulted by the secondary star just before periastron. This is shown by a gap in the curves in Fig. 10. At $i = 90^\circ$ the primary star also occults the shock apex. On account of the large volume of any colliding winds X-ray emission these occultations are not expected to have any observational X-ray signatures. At inclinations $i \gtrsim 30^\circ$ the maximum value of the circumstellar column becomes more asymmetric, and shifts in phase to where the shock apex is ‘behind’ the primary (i.e. $\phi \sim 0.15$ – see Fig. 9). The orbital inclination has just been recalculated to lie in the range $i = 50 - 70^\circ$ (c.f. Marchenko et al. 2000).

Comparing these results with the fitted columns in Table 3 is difficult, although they are of the correct order of magnitude. Assuming an ionized wind temperature of $\sim 10^4$ K, the $\tau = 1$ optical depth surface occurs at $N_H \sim 2 \times 10^{21} \text{ cm}^{-2}$ and $N_H \sim 6 \times 10^{21} \text{ cm}^{-2}$ for 0.5 and 1.0 keV photons respectively (c.f. for example, Krolick & Kallman 1984). This difference is mostly due to the Oxygen K-edge. Thus as Fig. 10 shows, the wind is indeed largely transparent at both of these energies, and for realistic values of the mass-loss rates. Only at phases near $\phi = 0.0$, where $N_H \sim 10^{22} \text{ cm}^{-2}$, does the absorption begin to become appreciable (this is one of the causes of the X-ray minima in Figs. 11 and 13). We therefore face two hard questions. Firstly, given the near transparency of the wind throughout most of the orbit, why don’t we see the intrinsic variation in the colliding winds X-ray luminosity? Secondly, why do we not see enhanced absorption in our periastron observation? In the hope of providing satisfactory answers to these questions we have calculated the expected colliding winds X-ray emission from a complicated hydrodynamical model, as detailed in the following section.

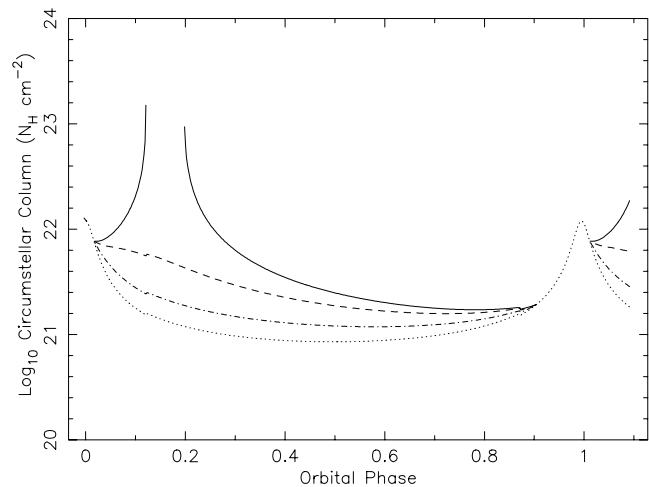


Figure 10. Circumstellar column to the colliding winds shock apex as a function of orbital phase for the same stellar parameters as used for model cw_1. The inclination of Iota Orionis is not well known so we show results for 4 sets of inclination (solid: $i = 90^\circ$; dash: $i = 60^\circ$; dot-dash: $i = 30^\circ$; dot: $i = 0^\circ$). The latest observational determination puts it at between 50 and 70° (Marchenko et al. 2000). Gaps in the curves indicate stellar occultation.

4.2 The cw_1 and cw_2 models

In this section we investigate in greater depth whether a colliding winds model *can* be consistent with the lack of variability in the characteristic temperature and count rate of the ASCA data and the unremarkable X-ray luminosity of this system. In particular, we have two questions: i) is the X-ray luminosity from the wind collision low enough that the expected phase variability is lost in the intrinsic background; ii) are radiative braking effects stronger than anticipated and can they provide an explanation for both the low luminosity and the constant X-ray temperatures.

Hydrodynamical models of the wind collision in Iota Orionis with $\eta = 31$ and 72 (with terminal velocity values input as v_1 and v_2) were presented in Pittard (1998). These simulations included the realistic driving of the winds by the radiation field of each star by using the line-force approximations of Castor, Abbott & Klein (1975). This approach allows the dynamics of the winds and radiation fields to be explored, and a number of interesting and significant effects have been reported (e.g. Stevens & Pollock 1994; Gayley, Owocki & Cranmer 1997, 1999). We refer the reader to these papers for a fuller discussion.

In Pittard (1998) it was found that the colliding winds shock always collapsed down onto the surface of the secondary star during periastron passage. On the other hand, there were large differences in the dynamics of the shock throughout the rest of the orbit. For model cw_2 the shock remained collapsed throughout the entire orbit, whilst for model cw_1 the shock lifted off the surface of the secondary as the stars approached apastron, before recollapsing as the orbit headed back towards periastron. However, due to the necessary simplifications we cannot be sure that the shock actually behaves in this manner for a system corresponding to the particular parameters used (we also reiterate the interpretation of the latest optical data by Marchenko et

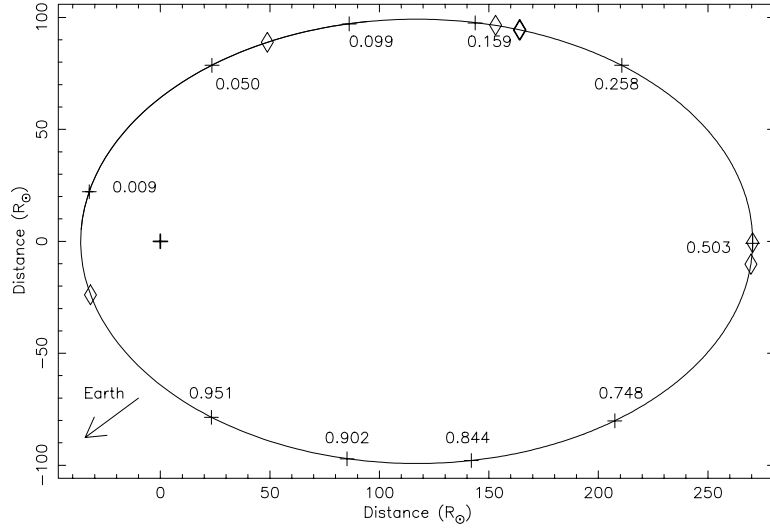


Figure 9. The assumed orbit in the frame of reference of the primary (marked with a cross at 0,0) for the cw_1 model. The direction of Earth is marked with an arrow. At periastron the line of sight into the system may be through the secondary wind for a very short period. This is mainly dependent on the inclination angle of Iota Orionis, which is poorly known. The phases, ϕ , over which the *ASCA* and *ROSAT* exposures were made are delineated by diamonds. Also indicated are the phases corresponding to the images in Fig. 1 of Pittard (1998) and the lightcurve in Fig. 13.

al. (2000) who suggest that the shock appears to be detached even at $\phi = 0.0 - 0.1$). Nevertheless, by comparing the orbital variation of the X-ray emission from these models with the (lack of) observed variability by *ASCA* we may be able to determine if the observed emission is consistent with a colliding winds origin and if so whether the collision shock is actually detached from the secondary star near apastron. We refer the reader to Pittard & Stevens (1997) for specific details of the X-ray calculation from the hydrodynamic models. We note that an orbital inclination of $i = 47^\circ$ was assumed for these calculations (c.f. Gies et al. 1996), and we do not expect them to change significantly in the light of the latest optical determination ($i = 50 - 70^\circ$, Marchenko et al. 2000).

4.3 An intrinsic wind shock interpretation

Fig. 11 shows the attenuated luminosity from model cw_2 as a function of phase. Immediately apparent is its low overall level in comparison to the *ROSAT* measured luminosity ($L_x \sim 2.0 \times 10^{32} \text{ erg s}^{-1}$). This gives us our first important insight into this system – the mass-loss rates of the two stars may be low enough with respect to other colliding wind systems that the resulting emission is washed out against the intrinsic background. If this is indeed the case one would not even expect to notice the severe drop in the colliding winds emission predicted by the model around periastron. Similarly one would not expect to notice the variation in the characteristic temperature of the interaction region shown in Fig. 12. We conclude, therefore, that the colliding winds X-rays may be so weak that they are washed out by a relatively constant component from the intrinsic X-rays from each wind. However, we need to be sure that the emission measure of this intrinsic component (EM_{wind}) is comparable to the X-ray observations (EM_{X-ray}), since if we lower

\dot{M} , we lower EM_{wind} and could run into the problem where $EM_{wind} < EM_{X-ray}$. EM_{wind} can be calculated from:

$$EM_{wind} = \int_{r=R_{min}}^{r=R_{max}} 4\pi r^2 \rho^2(r) f(r) dr, \quad (4)$$

where $f(r)$ accounts both for the volume filling factor and the differences in density of the shocked material relative to the ambient wind density $\rho(r)$ (which assumes a smooth wind, given by $\rho \equiv \dot{M}/4\pi r^2 v$). Previous wind instability simulations (Owocki et al. 1988; Owocki 1992; Feldmeier 1995) are broadly consistent with a constant or slowly decreasing filling factor as a function of radius (although details of the wind dynamics are still largely unknown). Feldmeier et al. (1997a) further argue that due to the processes of shock merging and destruction a monotonically decreasing or roughly constant filling factor is appropriate. Hence, in the following a constant f will be supposed. For an instability generated shock model, X-ray emission is only expected once the wind has reached a substantial fraction ($\gtrsim 50$ per cent) of v_∞ . We shall therefore take $R_{min} = 1.5R_*$. This is also sensible given that the observed X-ray flux doesn't show variability – if the emission occurred too close to the star eclipses would occur. With this value we also note that the fraction of the shocked wind occulted by the stellar disc is small. Feldmeier et al. (1997b) have also demonstrated that the X-ray emission from radii greater than $30R_*$ is negligible, so we take this as our upper bound, R_{max} . This is again reinforced by the fact that in Table 3, $N_H > N_{ISM}$. Equn. 4 then becomes $EM_{wind} = f \times EM_{smooth}$, where EM_{smooth} is the emission measure of the smooth wind evaluated between R_{min} and R_{max} .

Derived filling factors for the shock-heated gas are of order 0.1–1.0 per cent for O-stars (Hillier et al. 1993), but may possibly approach unity for near-MS B-stars (Cassinelli et al. 1994). For model cw_1, $EM_{smooth} = 7.6 \times 10^{56} \text{ cm}^{-3}$

(assuming the velocity law in Equn. 1 with $\beta = 0.8$). When compared to the values of EM_{X-ray} in Table 3 we see that we require $f \sim 0.001 - 0.42$. For model cw_2, $EM_{smooth} = 3.0 \times 10^{56} \text{ cm}^{-3}$, and we require $f \sim 0.02 - 1.07$. Despite the large ranges these are compatible with the observations (given that they also include the difference in density between the shocked material and a smooth wind), and therefore are consistent with an intrinsic wind shock interpretation.

However, a possible problem with this interpretation arises from the larger flux seen in the *ROSAT* spectrum at soft energies with respect to the *ASCA* spectra. If we believe that the spectral model parameters from the *ROSAT* and *ASCA* data are inconsistent, and that the variation in circumstellar attenuation is negligible, then this must be due to a real change in the intrinsic flux. This appears somewhat untenable though, given the overall lack of variability in single O-stars.

4.4 A colliding winds interpretation

In Fig. 13 we show the X-ray lightcurve from model cw_1. This time the colliding wind emission is much stronger (owing to the higher mass-loss rates assumed – see Table 5), and is again very variable. At the phases corresponding to the *ASCA* data the synthetic lightcurve is at local minima, and consistent with the observed luminosity[‡]. The model lightcurve also predicts that the observed luminosity at phase $\phi = 0.17$ should be higher than those at phases $\phi = 0.0$ and 0.5 , with the latter at roughly the same level[§]. From Table 3 we indeed find that this is the case, with the *ROSAT* luminosity matching the predicted lightcurve almost exactly[¶]. One slight worry is that the two *Einstein* observations at phases $\phi \sim 0.90$ and 0.97 do not show a significant enhancement in count rate with respect to the observation at phase $\phi = 0.59$. It would therefore be clearly useful to obtain new observations at these phases.

The orbital variation of the characteristic temperature fitted to the colliding winds region of model cw_1 is shown in Fig. 14. Our best estimate of the temperature varies from ~ 0.2 keV at periastron to $\sim 0.3 - 0.4$ keV at apastron. This temperature variation is much less than expected from a simple consideration of the variation of the pre-shock velocities along the line-of-centres, and reflects the fact that the fitted temperature is an average over the entire post-shock region. The temperatures predicted by the model are comparable with the observed data and we thus conclude that

[‡] We note that the equations of Usov (1992) give un-attenuated luminosities roughly an order of magnitude below the results of our numerical calculations.

[§] There is some uncertainty in the true luminosity during the periastron passage because the assumption of axisymmetry is poor at these phases, and additionally the optical data suggests that the wind collision region does not collapse onto the surface of the secondary.

[¶] We note that the quoted GIS L_x ($\phi = 0.5$) is much higher than the GIS L_x ($\phi = 0.0$) value. We conclude that this is due to uncertainties in the spectral fit parameters because the GIS background subtracted count rates are nearly identical from Table 2.

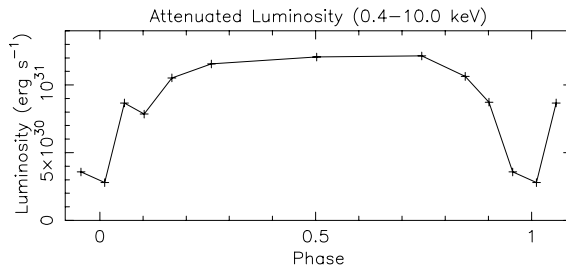


Figure 11. The 0.4–10.0 keV attenuated lightcurve for the colliding wind model cw_2. A large drop in the emission around periastron is clearly seen.

this model demonstrates that the observed emission does not allow us to discard a colliding winds interpretation.

4.5 Other possibilities/factors

Another intriguing possibility is that radiative braking in the Iota Orionis system is actually quite efficient (more so than the predictions of both models cw_1 and cw_2). This might also explain the inference of Marchenko et al. (2000) that the shock is lifted off the surface of the secondary around periastron. This would require strong coupling between the B-star continuum and the primary wind, but cannot be ruled out by our present understanding. In the adiabatic limit (which is a good approximation for the wind collision in Iota Orionis at apastron), Stevens et al. (1992) determined that

$$L_x \propto \dot{M}^2 v^{-3.2} D^{-1} (1 + \sqrt{\eta}) / \eta^2, \quad (5)$$

where it was assumed that the temperature dependence of the cooling curve was $\Lambda \propto T^{-0.6}$. This latter assumption is appropriate for post-shock gas in the temperature range $\sim 10^5 - 10^7$ K, which corresponds to pre-shock velocities of up to $\sim 1000 \text{ km s}^{-1}$ for solar abundance material. (Note: there is a typographical error in the corresponding equation of Stevens & Pollock, 1994). Assuming that η is small (i.e. that the wind of the primary dominates) we then find that to first order, $L_x \propto v^{-1.2}$. Thus the X-ray luminosity is almost inversely proportional to the pre-shock velocity of the primary wind. A reduction of 10 (50) per cent in the latter leads to an increase in the emission of 13 (130) per cent. Conversely, we find from the equations in Usov (1992), that $L_x \propto v^{-5/2}$ for the shocked primary wind and $L_x \propto v^{1/2}$ for the shocked secondary wind. For model cw_1 the emission from the latter appears to be dominant. Hence, for the same variations in the pre-shock velocity as discussed above, the emission is *reduced* by 5 and 30 per cent respectively. The discrepancy between these two sets of results is due to the different assumptions on the form of the cooling curve. Usov (1992) assumed cooling dominated by bremsstrahlung (i.e. $\Lambda \propto T^{1/2}$), which is more appropriate at higher temperatures ($T > 10^7$ K). Clearly then, the situation is rather confusing at present, not least because the *actual* position of the colliding wind region relative to the two stars is very poorly known, as is the relative mass-loss rates of the stars. It is therefore difficult for us to be any more quantitative without performing a rigorous parameter-space study.

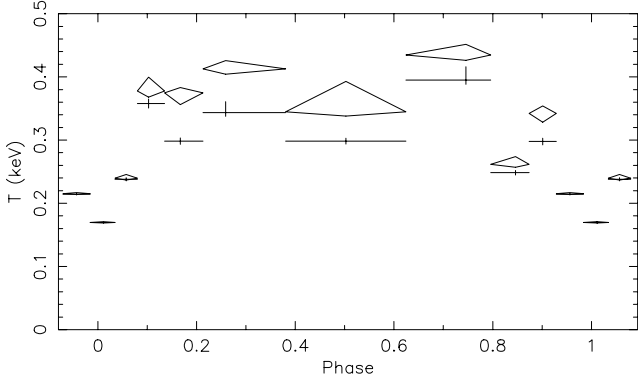


Figure 12. The orbital variation of the characteristic temperature from a one-temperature RS model fitted to the colliding wind model cw_2. Fits assuming solar abundance are marked with crosses, and those with a global floating abundance are marked with diamonds. A minimum in the characteristic temperature around periastron is clearly seen, reflecting the reduced pre-shock velocity of the primary wind in the hydrodynamical model.

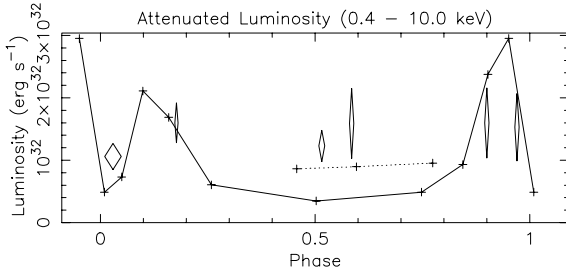


Figure 13. The 0.4–10.0 keV attenuated lightcurve for the colliding wind model cw_1. The small crosses (joined by the solid line) were calculated from the frames in Fig. 1 of Pittard (1998) at the phases indicated on Fig. 9. A large drop in the emission around periastron is clearly seen. However, when the shock detaches from the secondary in this model a much larger grid is required to ‘capture’ all of the X-ray emission – this is shown by the dotted line. Also marked on this figure are the observed luminosities from the *ASCA* and *ROSAT* pointings. The uncertainty in the count rates is a minimum of 1.2 per cent for the SIS0 periastron data, rising to a maximum of 4.3 per cent for the GIS2 apastron data. However, due to the uncertainties in the spectral shapes we conservatively assume a ± 20 per cent error in their resultant luminosities. A very good fit is obtained if one retains a healthy scepticism about the exact size of the periastron minimum in the model, where our assumption of axisymmetry is least valid. We also mark on the relative count rates of the three *Einstein* observations reported by Snow, Cash & Grady (1981). Because the conversion from count rate to luminosity is poorly known for these observations we have assumed uncertainties of ± 35 per cent and arbitrarily adjusted their scaling to best fit our model curve.

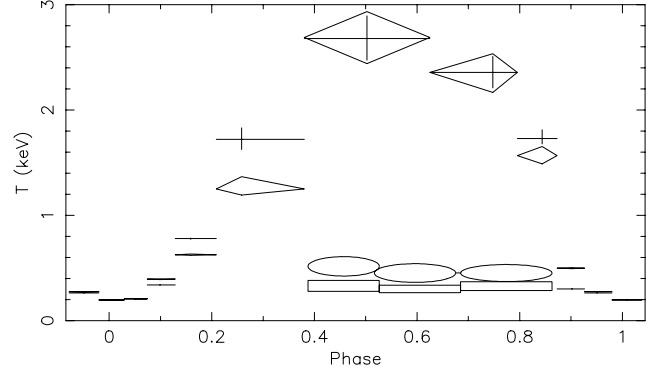


Figure 14. The orbital variation of the characteristic temperature from a one-temperature RS model fitted to the colliding wind model cw_1. Fits assuming solar abundance are marked with crosses, and those with a global floating abundance are marked with diamonds. A minimum in the characteristic temperature around periastron is clearly seen, reflecting the reduced pre-shock velocity of the primary wind in the hydrodynamical model. Note that unrealistically high values (> 1 keV) are obtained over the range $0.2 \lesssim \phi \lesssim 0.9$ due to the grid not capturing all of the emission. The rectangles and ellipses show the correct results of solar and floating abundance fits to a larger hydrodynamical grid over this phase range. Thus the characteristic temperature is within the range 0.2 – 0.4 keV over the *entire* orbital phase.

It is also possible that the characteristics of the emission may be altered by other physical processes. In investigating how electron thermal conduction may affect colliding wind X-ray emission, Myasnikov & Zhekov (1998) discovered that pre-heating zones in front of the shock have the overall effect of increasing the density of the wind interaction region. The resulting X-ray emission was found to change markedly, with a large increase in luminosity and a significant softening of the spectrum. Softer X-rays suffer significantly higher absorption so the resulting observed emission may have an unremarkable luminosity. Whether the observed emission would show orbital variability is not clear at this stage.

Finally, complex mutual interactions between the various physical processes occurring in colliding winds systems may also significantly alter the resultant emission. For instance, Folini & Walder (2000) suggest that the effects of thermal conduction and radiative braking may positively reinforce each other. We are a long way from performing numerical simulations which would investigate this.

5 COMPARISON WITH OTHER COLLIDING WIND SYSTEMS

Most early-type systems with strong colliding wind signatures are WR+OB binaries. These are different from OB+OB systems in a number of ways which may explain why it appears that stronger colliding wind signatures are obtained from WR+OB systems. First, the high values of \dot{M}_{WR} provide more wind material which can be shocked. Second, the spectral emissivity for WC wind abundances is greater than that for solar abundances at the same mass-density (i.e. mass-loss rate – see Stevens et al. 1992). How-

ever, both of these points may also act in reverse (high mass-loss rates also provide more absorption, and the emissivity of WN wind abundances for a given mass density is below that of solar). At this point it is therefore instructive to compare the X-ray characteristics of Iota Orionis with other early-type binary systems. The latter can be subdivided into three distinct groups as detailed in the following subsections.

5.1 Those with strong colliding winds signatures

Into this group fall the well-known binaries WR 140 (HD 193793) and γ^2 Velorum (WR 11, HD 68273). Both these systems show clear evidence for colliding stellar winds including phase-variable emission and a hard spectrum. WR 140 (WC7 + O4-5, $P=7.94$ yr) is famous for its episodic dust formation during periastron passage (Williams 1990). Strong X-ray emission from WR 140 was discovered by *EXOSAT* and its progressive extinction with phase by the WC7 wind has been used to derive the CNO abundances of the WR wind (Williams et al. 1990). Possible non-thermal X-ray emission has also recently been discovered in this system, as witnessed by the variability of the Fe K line (Pollock, Corcoran & Stevens 1999).

ROSAT observations of γ^2 Velorum (WC8 + O9I, $P=78.5$ d) were presented by Willis, Schild & Stevens (1995). The hard X-ray flux showed a phase repeatable increase by a factor of 4 when the system was viewed through the less-dense wind of the O-star, which was attributed to the addition of a harder component to the largely unvarying softer emission. More recent *ASCA* observations (Stevens et al. 1996, and a re-analysis by Rauw et al. 2000) confirmed these results. A detailed comparison of this data with synthetic spectra generated from a grid of hydrodynamical colliding wind models provided evidence that the hard X-ray emission comes directly from the wind collision.

5.2 Those showing some evidence of colliding winds

The best example of this category is V444 Cyg (WR 139, HD 193576), a well-studied eclipsing WN5 + O6 binary with an orbital period $P=4.21$ d and well known physical parameters. Corcoran et al. (1996) confirmed from phase-resolved *ROSAT* observations that although the luminosity was 1–2 orders of magnitude lower than the predictions of Stevens et al. (1992), there was an orbital dependence of the flux. This on its own did not completely rule out the O-star being the source of the X-rays, though fairly convincing evidence for colliding winds remained. First, the high value of the characteristic temperature outside of eclipse ($kT \sim 1.7$ keV) was much greater than the typical temperatures of single O-stars ($kT \sim 0.5$ keV). Second, the variation of the emission was consistent with a shock location near the O-star surface, as would be expected given the higher mass-loss rate of the WR-star and previous deductions from ultraviolet *IUE* observations (Shore & Brown 1988). Finally, the assumption of instantaneous terminal wind velocity overestimates the observed X-ray luminosity. More recent *ASCA* (Maeda et al. 1999) and optical (Marchenko et al. 1997) observations of this system have reinforced this interpretation.

However, some puzzling X-ray characteristics remain such as large amplitude short time-scale variability which is not easily explained by a colliding winds model (Corcoran et al. 1996).

Another system which shows some, but not overwhelming, characteristics of colliding winds is 29 UW Canis Majoris (HR 2781; HD 57060). This is also a short-period ($P=4.3934$ d) eclipsing binary system. *ROSAT* X-ray observations presented by Berghöfer & Schmitt (1995b) showed phase-locked variability with a single broad trough centered near secondary minimum. However a colliding winds interpretation was dismissed by the authors on the assumption that the wind momenta of the component stars were broadly similar and thus that the shocked region was nearly planar (Wiggs & Gies 1993). Such a scenario should form a double-peaked lightcurve (e.g. Pittard & Stevens 1997) and the majority of the emission was therefore attributed to the secondary's wind. The unremarkable X-ray luminosity also seemed in accordance with single O-star emission. However, if the wind momenta are much more imbalanced than believed, the lightcurve *would* be expected to have a single broad minimum, in agreement with the observations. HD 57060 also suffers from the Struve-Sahade effect (Stickland 1997; Gies, Bagnuolo & Penny 1997), and whilst the cause of this remains uncertain, colliding stellar winds is one possible interpretation. We therefore conclude that colliding winds may still be significant in this system.

Other strong candidates for colliding winds emission include HD 93205 and HD 152248 (c.f. Corcoran 1996), both of which are due to be observed with the *XMM* satellite, and HD 165052 (see Pittard & Stevens 1997 for more details).

5.3 Those with no colliding winds signature

Many early-type binaries observed by X-ray satellites show no signature of colliding winds emission. For the most part this is because the observations are generally short, the lightcurves extremely sparse and the expected luminosities near or below previous detection limits. However, one fairly bright frequently observed system which shows no signs whatsoever of colliding winds emission is δ Orionis A (HD 36486), a spectroscopic and eclipsing binary (O9.5 II + B0 III) with a 5.7 day period. As far as we know there has been no published paper which specifically investigates any potential colliding winds emission in this system.

6 CONCLUSIONS

In this paper we have analysed two *ASCA* X-ray observations of the highly eccentric early-type binary Iota Orionis, which were taken half an orbit apart at periastron and apastron. Although all previous observations were short and without good phase coverage, it was expected that a strong colliding winds signature would be seen. This expectation was based on the almost order of magnitude variation in the orbital separation between these phases and the known dependence of the X-ray luminosity of colliding winds (and suspected dependence of the spectral shape) with this. In turn it was hoped that this would reveal further insight into the physics of radiative driving and stellar winds from

Table 6. Summary of the strengths and weaknesses of the two interpretations of the X-ray emission considered.

	Intrinsic Wind Shocks	Colliding Winds
Pros	<p>Lack of variability in <i>ASCA</i> data.</p> <p>Low mass-loss rates of the stars can reduce CW emission but without running into problems with the X-ray emission measure exceeding that of the wind.</p>	<p>Lightcurve and spectra of model <i>cw_1</i> are consistent with the observational data, despite neither matching our initial simple expectations.</p>
Cons	<p>Circumstellar attenuation around periastron may be significant.</p>	<p>Modelling is very difficult and contains a number of assumptions and approximations.</p> <p>Optical data suggests that the wind collision shock does not crash onto the surface of the secondary during periastron passage.</p>

early-type stars, and in particular the additional interactions possible in binary systems. Indeed, Iota Orionis was selected as a target precisely because substantial changes were expected which would allow us to ‘probe’ the dynamics of the wind collision and infer the amount of radiative braking/inhibition.

Although our analysis was complicated by various problems experienced with the *ASCA* datasets, we found the emission to be surprisingly constant and unvarying between the two observations, in direct contradiction with our expectations. A further analysis of archival *ROSAT* data demonstrated a relatively low X-ray luminosity from this system of $L_x \sim 1.0 - 1.6 \times 10^{32} \text{ erg s}^{-1}$. Using a simple model we confirmed that the column along the line of sight to the expected position of the shock apex was unlikely to produce any significant attenuation of the shock X-rays, except perhaps around periastron. Based on an expected $1/D$ variation in the emission this did not help to explain our constant count rate, and subsequently significantly more complex hydrodynamical models were used to investigate the problem.

Despite strongly phase-variable emission from the models, both were consistent with the observations. The model with the lower mass-loss rates (*cw_2*) predicted attenuated luminosities an order of magnitude below the observational data, implying that intrinsic wind shocks emit the majority of the observed emission. On the other hand, the model with the higher mass-loss rates (*cw_1*) predicted minima in the colliding winds emission which coincided with the phases of the *ASCA* observations, and slightly enhanced emission at the phase of the *ROSAT* observation. This was also consistent with the data, implying that the observed emission could also be interpreted as purely colliding winds emission. In Table 6 we summarize the strengths and weaknesses of each of these.

Unfortunately it is impossible to distinguish between these two interpretations with the limited dataset currently available. Additional observations are clearly needed. New data with increased spatial resolution (to avoid source confusion from objects such as NSV 2321), spectral resolution

and counts (to constrain spectral and luminosity variability), and phase coverage is necessary if we are to begin distinguishing the competing interpretations. Observations at other wavelengths to further refine the system parameters (particularly the mass-loss rates of *both* stars) are also desirable.

Finally we compare the Iota Orionis observations with those obtained for other early-type binary systems. Although Iota Orionis is not the first well-studied early-type binary to show no *clear* signature of colliding winds emission (δ Orionis A is another), it *is* the first binary with a highly eccentric orbit not to do so. The lack of a clear colliding winds signature in Iota Orionis makes it noticeably different from other eccentric binaries (e.g. WR 140, γ^2 Velorum) where such signatures are readily seen at X-ray energies. Thus, Iota Orionis raises new open questions in our understanding of early-type binaries. In particular, we would like to know why the colliding winds emission is not obvious in Iota Orionis. Is it simply a result of the low mass-loss rates, a particular combination of system parameters, or are there deeper forces at work? This may be the first indication of the importance of radiative braking on a line-driven wind.

Acknowledgments

We thank the *XMEGA* group for the opportunity of analysing the *ASCA* datasets and John Blondin for the use of VH-1. In particular we would like to acknowledge some very helpful comments from various members of the *XMEGA* group. We acknowledge the use of the Birmingham and Leeds *Starlink* nodes where the calculations were performed. We are indebted to the developers and maintainers of the X-ray packages XSPEC and XSELECT, distributed by HEASARC, and of ASTERIX, distributed by PPARC. JMP gratefully acknowledges funding from the School’s of Physics & Astronomy at Birmingham and Leeds, and IRS acknowledges funding of a PPARC Advanced Fellowship. This research has made use of the SIMBAD astronomical

database at the CDS, Strasbourg. Finally we would like to thank the referee whose constructive comments greatly improved this paper.

REFERENCES

- Berghöfer T.W., Schmitt J.H.M.M., 1995a, *Adv. Space Res.*, 16, 163
- Berghöfer T.W., Schmitt J.H.M.M., 1995b, In: K.A. van der Hucht and P.M. Williams (eds.), *Wolf-Rayet Stars: Binaries; Colliding winds; Evolution*, Proc. IAU Symposium No. 163 (Kluwer Academic Publishers; Dordrecht), p. 382
- Berghöfer T.W., Schmitt J.H.M.M., Danner R., Cassinelli J.P., 1997, *A&A*, 322, 167
- Caillault J.-P., Gagné M., Stauffer J.R., 1994, *ApJ*, 432, 386
- Cassinelli J.P., Cohen D.H., MacFarlane J.J., Sanders W.T., Welsh B.Y., 1994, *ApJ*, 421, 705
- Castor J.I., Abbott D.C., Klein R.I., 1975, *ApJ*, 195, 157
- Chlebowski T., Harnden F.R. Jr., Sciortino S., 1989, *ApJ*, 341, 427
- Collura A., Sciortino S., Serio S., Vaiana G.S., Harnden F.R. Jr., Rosner R., 1989, *ApJ*, 338, 296
- Corcoran M.F., 1996, *RMAA Conf. Ser.*, 5, 54
- Corcoran M.F., et al., 1994, *ApJ*, 436, L95
- Corcoran M.F., Stevens I.R., Pollock A.M.T., Swank J.H., Shore S.N., Rawley G.L., 1996, *ApJ*, 464, 434
- Eichler D., Usov V.V., 1993, *ApJ*, 402, 271
- Feldmeier A., 1995, *A&A*, 299, 523
- Feldmeier A., Kudritzki R.-P., Palsa R., Pauldrach A.W.A., Puls J., 1997a, *A&A*, 320, 899
- Feldmeier A., Puls J., Pauldrach A.W.A., 1997b, *A&A*, 322, 878
- Folini D., Walder R., 2000, *ASP Conf. Series*, submitted
- Gagné M., Caillault J.-P., 1994, *ApJ*, 437, 361
- Gagné M., Caillault J.-P., Stauffer J.R., 1995, *ApJ*, 445, 280
- Gayley K.G., Owocki S.P., Cranmer S.R., 1997, *ApJ*, 475, 786
- Gayley K.G., Owocki S.P., Cranmer S.R., 1999, *ApJ*, 513, 442
- Geier S., Wendker H.J., Wisotzki L., 1995, *A&A*, 299, 39
- Gies D.R., Bagnuolo W.G. Jr., Penny L.R., 1997, *ApJ*, 479, 408
- Gies D.R., Wiggs M.S., Bagnuolo W.G., Jr., 1993, *ApJ*, 403, 752
- Gies D.R., Barry D.J., Bagnuolo W.G., Jr., Sowers J., Thaller M.L., 1996, *ApJ*, 469, 884
- Hillier D.J., Kudritzki R.P., Pauldrach A.W.A., Baade D., Cassinelli J.P., Puls J., Schmitt J.H.M.M., 1993, *A&A*, 276, 117
- Hwang U., Mushotzky R.F., Burns J.O., Fukazawa Y., White R.A., 1999, *ApJ*, 516, 604
- Koyama K., Maeda Y., Tsuru T., Nagase F., Skinner S.L., 1994, *PASJ*, 46, L93
- Krolick J.H., Kallman T.R., 1984, *ApJ*, 286, 366
- Kudritzki R.P., Palsa R., Feldmeier A., Puls J., Pauldrach A.W.A., 1996, *Proc. 'Röntgenstrahlung from the Universe'*, eds. Zimmermann H.U., Trümper J., Yorke, H., MPE Report 263, 9
- Long K.S., White R.L., 1980, *ApJ*, 239, L65
- Maeda Y., Koyama K., Yokogawa J., Skinner S., 1999, *ApJ*, 510, 967
- Marchenko S.V., Moffat A.F.J., Eenens P.R.J., Cardona O., Echevarria J., Hervieux Y., 1997, *ApJ*, 485, 826
- Marchenko S.V. et al. 2000, *MNRAS*, accepted
- McCaughrean M.J., Stauffer J.R., 1994, *AJ*, 108, 1382
- Moreno E., Koenigsberger G., 1999, *RMAA*, 35, 157
- Myasnikov A.V., Zhekov S.A., 1998, *MNRAS*, 300, 686
- Owocki S.P., 1992, In: U. Heber U., S. Jeffery (eds.), *The Atmospheres of Early-type Stars*, Springer, Heidelberg, p. 393
- Owocki S.P., Castor J.I., Rybicki G.B., 1988, *ApJ*, 335, 914
- Pittard J.M., 1998, *MNRAS*, 300, 479
- Pittard J.M., Stevens I.R., 1997, *MNRAS*, 292, 298
- Pollock A.M.T., Corcoran M.F., Stevens I.R., 1999, In: K.A. van der Hucht, G. Koenigsberger & P.R.J. Eenens (eds.), *Wolf-Rayet Phenomena in Massive Stars and Starburst Galaxies*, Proc. IAU Symposium No. 193 (San Francisco: ASP), p. 388
- Rauw G., Stevens I.R., Pittard J.M., Corcoran M.F., 2000, *MNRAS*, accepted
- Raymond J.C., Smith B.W., 1977, *ApJS*, 35, 419
- Savage B.D., Bohlin R.C., Drake J.F., Budich W., 1977, *ApJ*, 216, 291
- Shore S.N., Brown D.N., 1988, *ApJ*, 334, 1021
- Shull J.M., Van Steenberg M.E., 1985, *ApJ*, 194, 599
- Snow T.P. Jr., Cash W., Grady C.A., 1981, *ApJ*, 244, L19
- Stevens I.R., 1988, *MNRAS*, 235, 523
- Stevens I.R., Blondin J.M., Pollock A.M.T., 1992, *ApJ*, 386, 265
- Stevens I.R., Corcoran M.F., Willis A.J., Skinner S.L., Pollock A.M.T., Nagase F., Koyama K., 1996, *MNRAS*, 283, 589
- Stevens I.R., Pollock A.M.T., 1994, *MNRAS*, 269, 226
- Stickland D.J., 1997, *Observatory*, 117, 37
- Stickland D.J., Pike C.D., Lloyd C., Howarth I.D., 1987, *A&A*, 184, 185
- Strickland D.K., Stevens I.R., 1998, *MNRAS*, 297, 747
- Tanaka Y., Inoue H., Holt S.S., 1994, *PASJ*, 46, L37
- Usov V.V., 1992, *ApJ*, 389, 635
- Waldron W.L., 1991, *ApJ*, 382, 603
- Waldron W.L., Corcoran M.F., Drake S.A., Smale A.P., 1998, *ApJS*, 118, 217
- Warren, W.H. Jr., Hesser J.E., 1977, *ApJS*, 34, 115
- Wiggs M.S., Gies D.R., 1993, *ApJ*, 407, 252
- Willis A.J., Schild H., Stevens I.R., 1995, *A&A*, 298, 549
- Williams P.M., van der Hucht K.A., Pollock A.M.T., Florkowski D.R., van der Woerd H., Wamsteker W.M., 1990, *MNRAS*, 243, 662
- Yamauchi S., Koyama K., Sakano M., Okada K., 1996, *PASJ*, 48, 719